BUTTERWORTH HEINEMANN

*Polymer* Vol. 36 No. 12, pp. 2347–2354, 1995

0032-3861/95/$10.00 + 0.00

# Molecular motions of liquid crystalline polymers with various spacer lengths in the glass and nematic states

**Regan L. Silvestri* and Jack L. Koenig†**
*Department of Macromolecular Science, Case Western Reserve University, Cleveland, OH 44106, USA*

**and Wayne R. Likavec and William M. Ritchey**
*Department of Chemistry, Case Western Reserve University, Cleveland, OH 44106, USA*
*(Received 29 June 1994; revised 26 October 1994)*

A side-chain liquid crystalline polymer (LCP) based on the 4-hydroxy-4′-methoxy-α-methylstilbene mesogen attached through a flexible spacer of eight methylenic units to a poly(methyl acrylate) backbone is studied via solid-state $^{13}C$ nuclear magnetic resonance (n.m.r.) spectroscopy. The molecular dynamics in the MHz frequency regime are characterized as a function of temperature by the spin–lattice relaxation time constant $T_1$. Rotational correlation times ($\tau_c$s) and activation energies ($E_a$s) are calculated for motions at various local sites in the glass and nematic states. Rapid spinning of the methyl carbons occurs on the fast side of the $T_1$ minimum, and the activation energy does not change at the phase transition. The motional activation energies of all three sites in the mesogen are nearly equal, indicating that the motion is collective. The activation energy decreases for the mesogen carbons in the nematic state by a factor of six, as the LCP is no longer frozen. In the glassy state the activation energy of the α spacer carbon is nearly equal to that of the mesogen, while the β spacer carbon is 30 times more mobile. The spacer begins to function as a flexible free spacer at the β position. Further flexibility is introduced at the γ and δ positions. Likewise, in the nematic state the mobility increases in the spacer from the α position inward. The activation energy of the backbone increases in the nematic state, with the backbone acting as a viscous drag to the motion of the mesogen. A comparison is made between the LCP with a spacer of eight methylenic units and an analogous LCP with a spacer of three methylenic units. In the glass state, $E_a$ is larger for the motion of the mesogen, the α spacer carbon and the β spacer carbon, for the LCP with eight methylenic units.

**(Keywords: n.m.r. spectroscopy; liquid crystalline polymers; molecular motions)**

## INTRODUCTION

Side-chain liquid crystalline polymers (LCPs) consist of pendant groups with mesomorphic properties as side chains off of a main-chain polymer backbone[1]. $^{13}C$ nuclear magnetic resonance (n.m.r.) spectroscopy in the solid state can be used to study the motions of LCPs in many frequency regimes[2–4]. Motions in the MHz regime are particularly important in determining the properties of liquid crystalline polymers[4–6]. Therefore, for this reason there has been much interest in studying the MHz motions of LCPs[7–12].

Spin–lattice relaxation in the static magnetic field is stimulated by molecular motions in the MHz frequency regime[5,13]. The rate of spin–lattice relaxation is inversely related to the time constant $T_1$, which is most commonly measured by the method of inversion–recovery using the 180°–τ–90° pulse sequence shown in *Figure 1*. The magnetization, $M(t)$, as a function of the variable delay time, $t$, is given by the following:

$$M(t) = M_0[1 - 2\exp(-t/T_1)] \quad (1)$$

where $M_0$ is the inherent total magnetization in the absence of relaxation effects and $T_1$ is the time constant describing the rate of the exponential recovery[2]. It is common to fit a three-parameter equation as follows:

$$M(t) = M_\infty + (M_{t=0} - M_\infty)\exp(-t/T_1) \quad (2)$$

because the experimental data are rarely centred symmetrically about zero[14].

Due to the inherently strong nature of the dipolar interaction in solids, the dominant relaxation mechanism is dipole–dipole relaxation, particularly if the carbon is bound by a proton[12,15,16]. That is, $^{13}C$ relaxation is stimulated by fluctuations in the local dipolar field, where the local field is modulated by molecular motion. For a pure $^{13}C$–$^{1}H$ dipolar relaxation, $T_1$ is related to $J(\omega)$, the spectral density function, by the following expression:

$$\frac{1}{NT_1} = \frac{1}{10}\left(\frac{\gamma_H^2\gamma_C^2\hbar^2}{r_{C-H}^6}\right)[J_0(\omega_H - \omega_C) + 3J_1(\omega_C) + 6J_2(\omega_H + \omega_C)] \quad (3)$$

* Present address: PREDICT Technologies, 9555 Rockside Road, Cleveland, OH 44125, USA
† To whom correspondence should be addressed

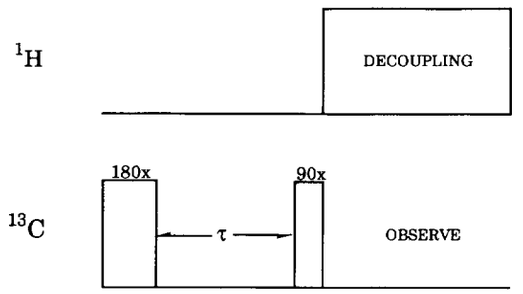


**Figure 1** $^{13}C$ n.m.r. pulse sequence used to measure $T_1$ via the inversion–recovery method

where $r_{C-H}$ is the internuclear carbon to hydrogen distance and $N$ is the number of bound protons[17]. The spectral density function, $J(\omega)$, is the Fourier inverse of the autocorrelation function. Assuming random isotropic reorientation of the C–H vector, the autocorrelation function is exponential with a time constant $\tau_c$, i.e. the rotational correlation time[2,3,17,18]. Therefore, the spectral density function is given by the following[2,3,17,18]:

$$J(\omega) = \tau_c/(1+\omega^2\tau_c^2) \quad (4)$$

Assuming pure dipolar relaxation (equation (3)) and random isotropic motion (equation (4)), the relaxation parameter $T_1$ can be related to $\tau_c$, the length of time between reorientations[19].

A plot of $T_1$ as a function of $\tau_c$ shows a minimum value of $T_1$ when $\omega_0 \simeq 1/\tau_c$ (see refs 3 and 4). On the fast side of the $T_1$ minimum the value of $T_1$ corresponding to a given $\tau_c$ is independent of $\omega$, whereas on the slow side of the minimum, $T_1$ is dependent on the strength of the static magnetic field[2–4,17].

For thermally activated motion, $\tau_c$ as a function of temperature is given by a simple Arrhenius expression, as follows:

$$\tau_c = \tau_0 \exp(E_a/RT) \quad (5)$$

where $E_a$ is the activation energy for motion and $R$ is the molar gas constant[9,20]. The activation energy is the barrier that must be overcome for reorientation to occur.

## EXPERIMENTAL

The side-chain LCP studied here is based on the 4-hydroxy-4′-methoxy-α-methylstilbene mesogen attached through a flexible spacer of eight methylenic units to a poly(methyl acrylate) backbone. This LCP, termed 4′-8-PMA and pictured in *Scheme 1*, has been previously synthesized and characterized by Percec and Tomazos[21].

Solid-state $^{13}C$ n.m.r. relaxation experiments were carried out on a Bruker MSL 300 spectrometer at a $^{13}C$ measuring frequency of 75.47 MHz and on a Bruker MSL 400 spectrometer at a $^{13}C$ measuring frequency of 100.627 MHz. All experiments were carried out with gated high-powered dipolar decoupling (GHPD), magic-angle spinning (MAS) at 3 kHz, and quadrature phase detection. The recycle delay between pulse sequence repetitions ($T_R$) was 10 s.

Using the 180°–τ–90°–ACQ–$T_R$ pulse sequence shown in *Figure 1*, values of $^{13}C$ $T_1$ were determined at 75 and 100 MHz at various temperatures from 23.5 to 79°C, using a temperature controller which was accurate to 0.5°C. Typically, 1200 scans were signal averaged for each τ, and 11 variable delays were used, ranging from 5 ms to 11 s.

Samples were spun in 7 mm-outer-diameter zirconia rotors with Kel-F end-caps and the magic angle was set by maximizing the $^{79}Br$ peak intensities of KBr[22]. The radio frequency (r.f.) fields ranged from 41 to 49 kHz, as calculated from the length of a 90° pulse. The 90° pulse length was determined from null intensities of adamantane at 360 and 720°. The chemical shift scale was set from the known peak positions of adamantane. Free induction decays (FIDs) with 512 to 1 K data points were collected and zero-filled to 8 K data points before Fourier transformation.

Peak intensities were measured without baseline correction and fitted to the three-parameter equation (equation (2)) to determine $T_1$. Curve fitting was carried out on a MicroVax III+ using a general non-linear least squares curve fitting program written in Fortran 77. The rotational correlation time, $\tau_c$, was calculated from $T_1$, according to equations (3) and (4), by using a binary search algorithm (also written in Fortran 77 on a MicroVax III+).

## RESULTS

Previously published differential scanning calorimetry (d.s.c.) and gel permeation chromatography (g.p.c.) data are given in *Table 1*[21]. The glass transition ($T_g$) is a second-order or kinetic transition. The temperature at which $T_g$ is observed depends on the frequency at which the measurement is taken[23,24]. As quantified by the Williams–Landel–Ferry equation[25], the glass transition is shifted upwards by ~10°C for each order of magnitude that the measuring frequency is increased[23,24]. D.s.c. has a measuring frequency of the order of Hz, and spin–lattice relaxation in the static field is stimulated by motions in the MHz frequency regime. Therefore, the glass transition will be observed approximately 60°C higher via n.m.r. inversion–recovery. Subsequent mesophase transitions and the isotropization are first-order transitions or thermodynamic transitions, and thus invariant with measuring frequency[23,24]. In the present case, shifting the

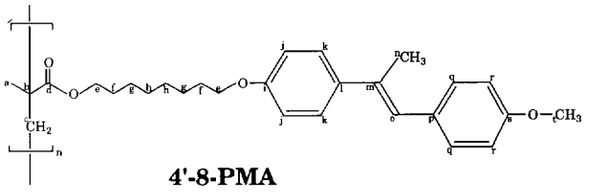

**4′-8-PMA**

**Scheme 1**

**Table 1** Transition temperatures (°C) as determined by d.s.c., with heating and cooling rates of 20°C min$^{-1}$, and molecular weights[a] as determined by g.p.c., for 4′-8-PMA (ref. 21)

| Transition | Heating | Cooling |
|---|---|---|
| $T_{g,s}$ | 18 | 15 |
| $T_{s,n}$ | 55 | 53 |
| $T_{n,i}$ | 112 | 108 |

[a] $M_n = 24.1 \times 10^3$; $M_w/M_n = 2.0$

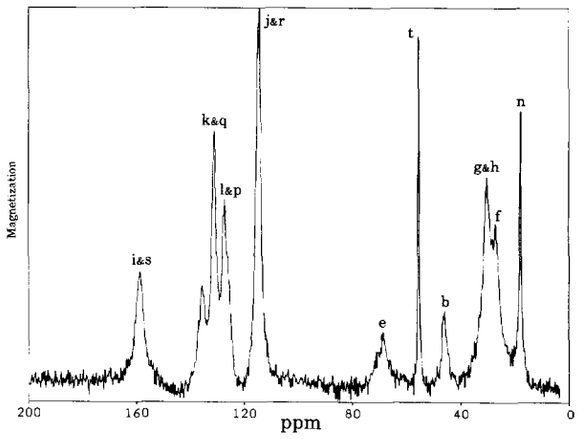


**Figure 2** Bloch decay/gated high-powered decoupling/magic-angle spinning 75 MHz $^{13}C$ n.m.r. spectrum of 4'-8-PMA at 79°C, showing peak assignments

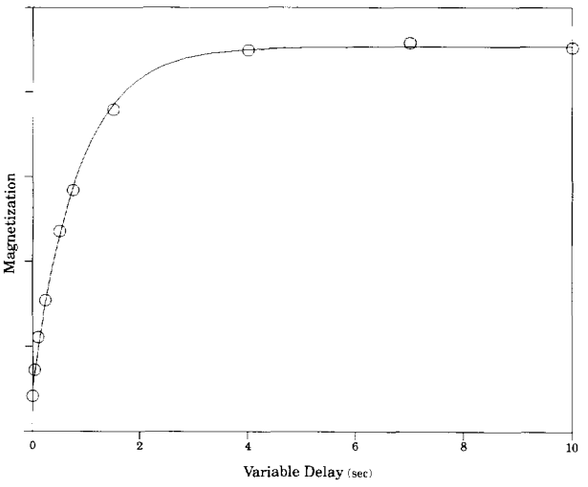


**Figure 3** A plot of the magnetization as a function of the variable delay time, using the 180°–τ–90° pulse sequence at 23.5°C for the peak at 114 ppm that has been assigned to $C_j$ and $C_r$

glass–smectic transition upwards by 60°C raises the glass transition above the smectic–nematic transition. Therefore, the smectic state is masked and the glassy state is observed up to the nematic transition.

Peak assignments are shown in *Figure 2*, where the letters correspond to the carbon subscripts as labelled in the chemical formula. Peak assignments were made by combining information from: (a) chemical shift calculations accounting for substituent effects[26,27], (b) known chemical shifts of model compounds, i.e. poly(methyl methacrylate)[28], methylstilbene, and linear ether–alkanes[26], (c) comparison with chemical shifts of other LCPs in the analogous series with different backbones and spacer lengths[5,6,29,30], (d) comparison with chemical shifts of the unpolymerized mesogen and mesogen with spacer[6], (e) spectral editing pulse sequences, and (f) quantitative n.m.r. peak areas.

A drastic decrease in chemical shift anisotropy is observed in the nematic state. Spinning sidebands were identified by acquiring spectra at different rates of magic-angle spinning. Given the high rate of the MAS, it can be assumed that nematic alignment is oriented along the spinning axis[31]. In addition, an increase in $T_2$ is observed in the nematic state. Cross polarization (CP) was found to be effective in the glassy state but ineffective in the nematic state. For this reason, all experiments were performed without CP in order to allow quantitative comparison between the glass and nematic states.

The Bloch decay pulse sequence with gated high-powered decoupling and magic-angle spinning was used to acquire spectra in going from the glassy state to the isotropic state. No change is observed in the chemical shifts of the methylene carbons, indicating no change in the ratio of *trans* to *gauche* isomers according to the *γ-gauche* effect[32,33].

*Figure 3* is a typical plot of the recovery of the inverted magnetization where equation (2) is fitted to the experimentally determined data points. Since unique $T_1$ values are obtained for each carbon it can be assumed that there is little or no $^{13}C$ spin diffusion[2].

*Variable temperature* $T_1$

*Figure 4* shows plots of $T_1$ as a function of inverse temperature for the various carbons at two static magnetic fields. Note that for the methyl carbons $C_n$ and $C_t$, $T_1$ at 100 MHz is equal to $T_1$ at 75 MHz over the entire temperature range. Since relaxation on the fast side of the $T_1$ minimum is independent of field[2–4,17], motion of the methyl carbons is on the fast side of the $T_1$ minimum in both the glass and nematic states. For all other carbons, $T_1$ at 100 MHz is larger than $T_1$ at 75 MHz, in the glassy state, while in the nematic state $T_1$ at 100 MHz is equal to $T_1$ at 75 MHz. Since relaxation on the slow side of the $T_1$ minimum is field dependent[2,4,17], the glassy polymer undergoes motions on the slow side of the minimum. Furthermore, since relaxation on the fast side of the $T_1$ minimum is independent of field[2–4,17], the nematic LCP undergoes motions on the fast side of the minimum.

Equations (3) and (4) are used to calculate $\tau_c$ from $T_1$. This calculation yields two possible values of $\tau_c$ for each $T_1$, i.e. one on each side of the minimum[3]. However, the variable field relaxation data are used to determine which of these $\tau_c$ values is correct. *Figure 5* plots the natural logarithm of $\tau_c$, as a function of inverse temperature, for the various carbons.

In the glassy state, $T_1$ is larger at 100 MHz than at 75 MHz because relaxation on the slow side of the minimum is field dependent. When the variable field values of $T_1$ are converted to values of $\tau_c$, it can be seen that $\tau_c$ is nearly independent of field. Assuming that the spectral density function is smooth[2–4], the density of motions at 100 MHz should be nearly equal to the density of motions at 75 MHz. Molecular motions vary greatly across the entire frequency spectrum; however, these two points are very close considering the wide range of motional frequencies.

At the phase transition, the correlation times increase discontinuously by three to four orders of magnitude. The motion of the nematic liquid crystal is three to four orders of magnitude faster than the glassy polymer. Note in particular that the $\beta$, $\gamma$ and $\delta$ spacer carbons ($C_f$, $C_g$ and $C_h$, respectively) all jump four orders of magnitude, while the $\alpha$ spacer carbon ($C_e$) jumps only three orders of magnitude. Directly following the nematic transition the $\alpha$ spacer carbon undergoes slower motions than the $\beta$, $\gamma$ and $\delta$ carbons, and the correlation times for the $\beta$, $\gamma$ and $\delta$ spacer carbons are nearly equal. With a continued

increase in temperature the $\alpha$ carbon eventually undergoes motions as fast as the $\beta$, $\gamma$ and $\delta$ carbons, but only after sufficient thermal energy has been applied. These observations will be further quantified in the discussion of the activation energies.

Linearizing the Arrhenius equation (equation (5)), activation energies are calculated from the slopes of the lines in *Figure 5*. However, when a carbon is not bound by a proton $r_{C\ H}$ may not be well defined and therefore it becomes difficult to calculate $\tau_c$. In this case, the

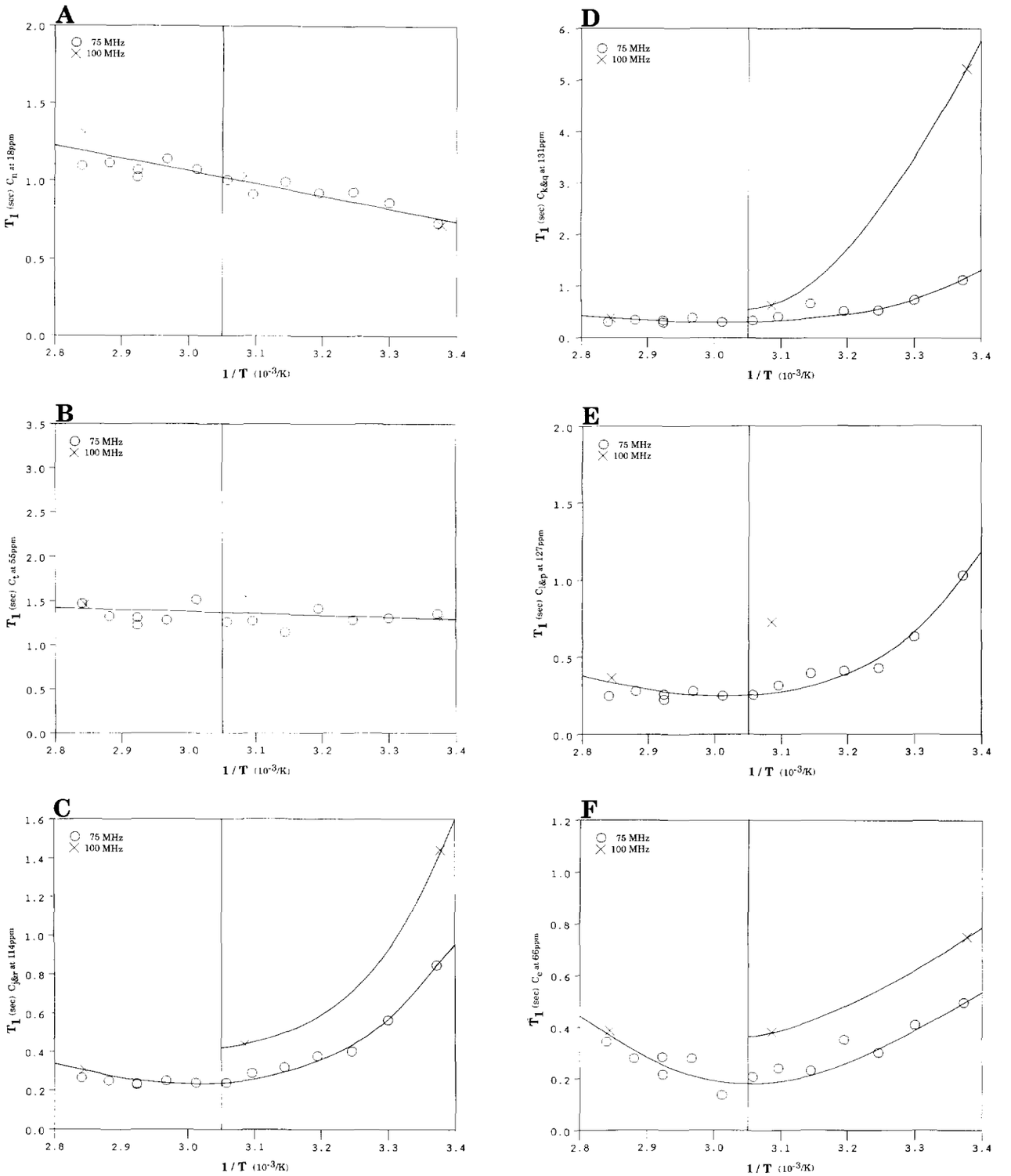


**Figure 4** Plots of $^{13}C$ $T_1$ as a function of inverse temperature at 75 and 100 MHz for (A) the peak at 18 ppm assigned to $C_n$, (B) the peak at 55 ppm assigned to $C_t$, (C) the peak at 114 ppm assigned to $C_j$ and $C_r$, (D) the peak at 131 ppm assigned to $C_k$ and $C_q$, (E) the peak at 127 ppm assigned to $C_l$ and $C_p$, (F) the peak at 66 ppm assigned to $C_e$, (G) the peak at 27 ppm assigned to $C_f$, (H) the peak at 30 ppm assigned to $C_g$ and $C_h$, and (I) the peak at 45 ppm assigned to $C_b$

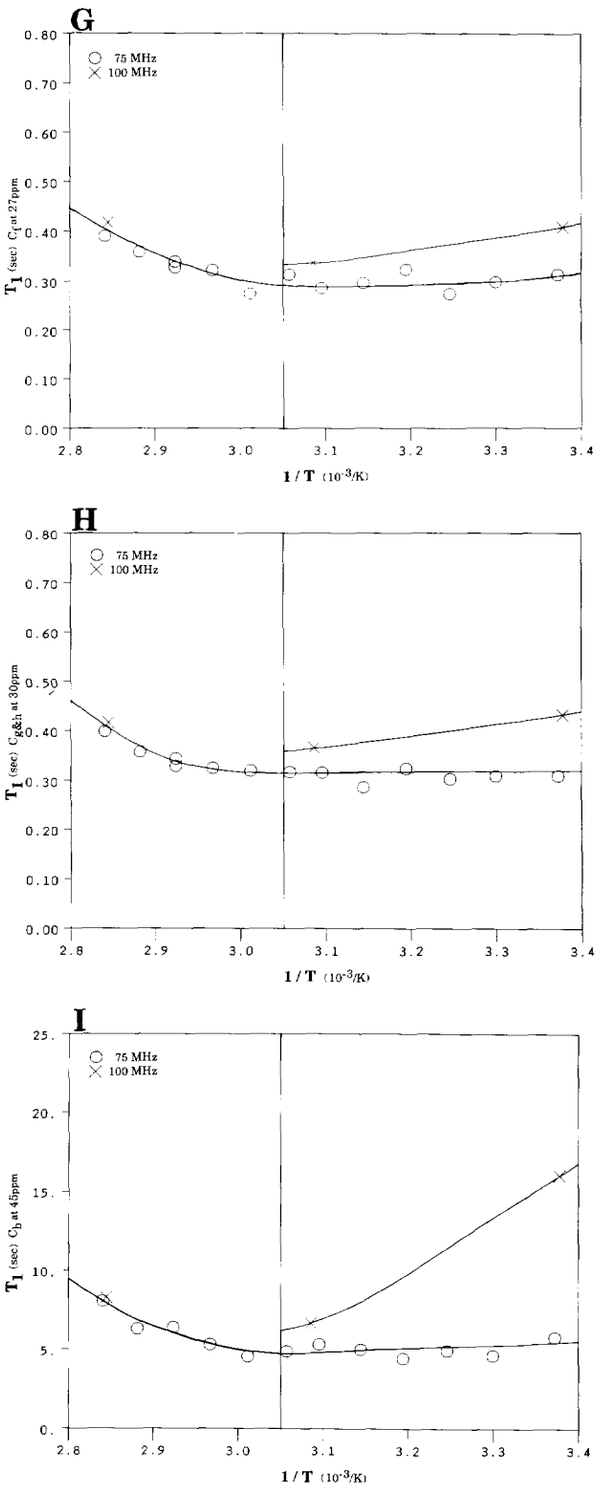


**Figure 4** *continued*

activation energy can be determined from the slope of a plot of $\ln(T_1)$ *versus* $1/T$, provided that no motions are near the $T_1$ minimum[34]. If the plot is in the linear portion on the slow side of the $T_1$ minimum then the slope is $E_a/R$. If the plot is in the linear portion on the fast side of the $T_1$ minimum then the slope is $-E_a/R$. Moreover, data from only one frequency can be used when determining the activation energy directly from $\ln(T_1)$ *versus* $1/T$, so the 100 MHz data are excluded.

The activation energies thus determined are listed in *Table 2*. Note that the activation energies change at the phase transition.

## DISCUSSION

Spin–lattice relaxation is sensitive to motions in the MHz frequency regime[3–5,13]. Even though the LCP is likely to be undergoing various motions throughout the frequency spectrum, only lattice motions at or near the Larmor frequency couple effectively with the decaying spin as it precesses in the static magnetic field. In the high-frequency MHz regime, short-range localized motions occur[5,23]. Internal reorientations (such as *trans–gauche* isomerizations and ring flips) are typical on such a fast time-scale[35].

### *Activation energies for methyl carbons*

For the methyl carbon $C_n$ at 18 ppm and the methoxy carbon $C_t$ at 55 ppm, motion is on the fast side of the $T_1$ minimum in both the glass and nematic states. The motion is certainly a rapid spinning of the methyl group about its $C_3$ axis. The activation energy for the spinning of a methyl group does not change at the phase transition, i.e. the spinning of a methyl group remains unchanged from the glass to the nematic state. However, the activation energy of the methoxy carbon $C_t$ is seven times less than that of $C_n$.

### *Activation energies for mesogen carbons*

Motional activation energies are determined at three sites in the mesogen, namely (a) the outermost protonated phenyl carbons, $C_j$ and $C_r$, at 114 ppm, (b) the innermost protonated phenyl carbons, $C_k$ and $C_q$, at 131 ppm, and (c) the substituted phenyl carbons bridging the two aromatic rings, $C_l$ and $C_p$, at 127 ppm. In the glassy state $E_a$ is almost equal for all three phenyl carbons. Similarly, in the nematic state $E_a$ is nearly equal at all three sites. This suggests that the motion is a collective motion of the entire phenyl group, possibly ring flipping about the *para*-axis. Ring flipping is the obvious motion to suggest in keeping with the thought that the only internal motions allowed in solids and liquids are symmetry operations[36,37].

Furthermore, the activation energy decreases by a factor of six in the nematic state. This transition marks the transition from a glassy polymer to a nematic liquid crystal, so it is not surprising that motion will require

**Table 2** Activation energies (±1%) for 4′-8-PMA in the glass and nematic states

| | | $E_a$ (kJ mol$^{-1}$) | |
|---|---|---|---|
| Carbon | ppm | Glass | Nematic |
| $C_n$ | 18 | 6.59 | 6.59 |
| $C_t$ | 55 | 0.922 | 0.922 |
| $C_j$, $C_r$ | 114 | 32.1 | 6.51 |
| $C_k$, $C_q$ | 131 | 39.4 | 4.87 |
| $C_l$, $C_p$ | 127 | 32.1 | 8.44 |
| $C_c$ | 66 | 21.1 | 39.7 |
| $C_f$ | 27 | 0.709 | 17.2 |
| $C_g$, $C_h$ | 30 | 0.587 | 12.7 |
| $C_b$ | 45 | 1.54 | 27.1 |

less energy. Indeed, the LCP is frozen in the glassy state and flows in the nematic state.

*Activation energies for spacer carbons*

Activation energies are determined at three localized sites in the spacer, namely (a) the spacer carbons $\alpha$ to the mesogen and to the backbone $C_e$ at 66 ppm, (b) the $\beta$ spacer carbons $C_f$ at 27 ppm, and (c) the $\gamma$ and $\delta$ spacer carbons, $C_g$ and $C_h$, respectively, overlapping at 30 ppm. In the glassy state the activation energy of the $\alpha$ spacer carbon $C_e$ is nearly equal to that of the mesogen. The $\beta$ spacer carbon $C_f$ is 30 times more mobile than the $\alpha$

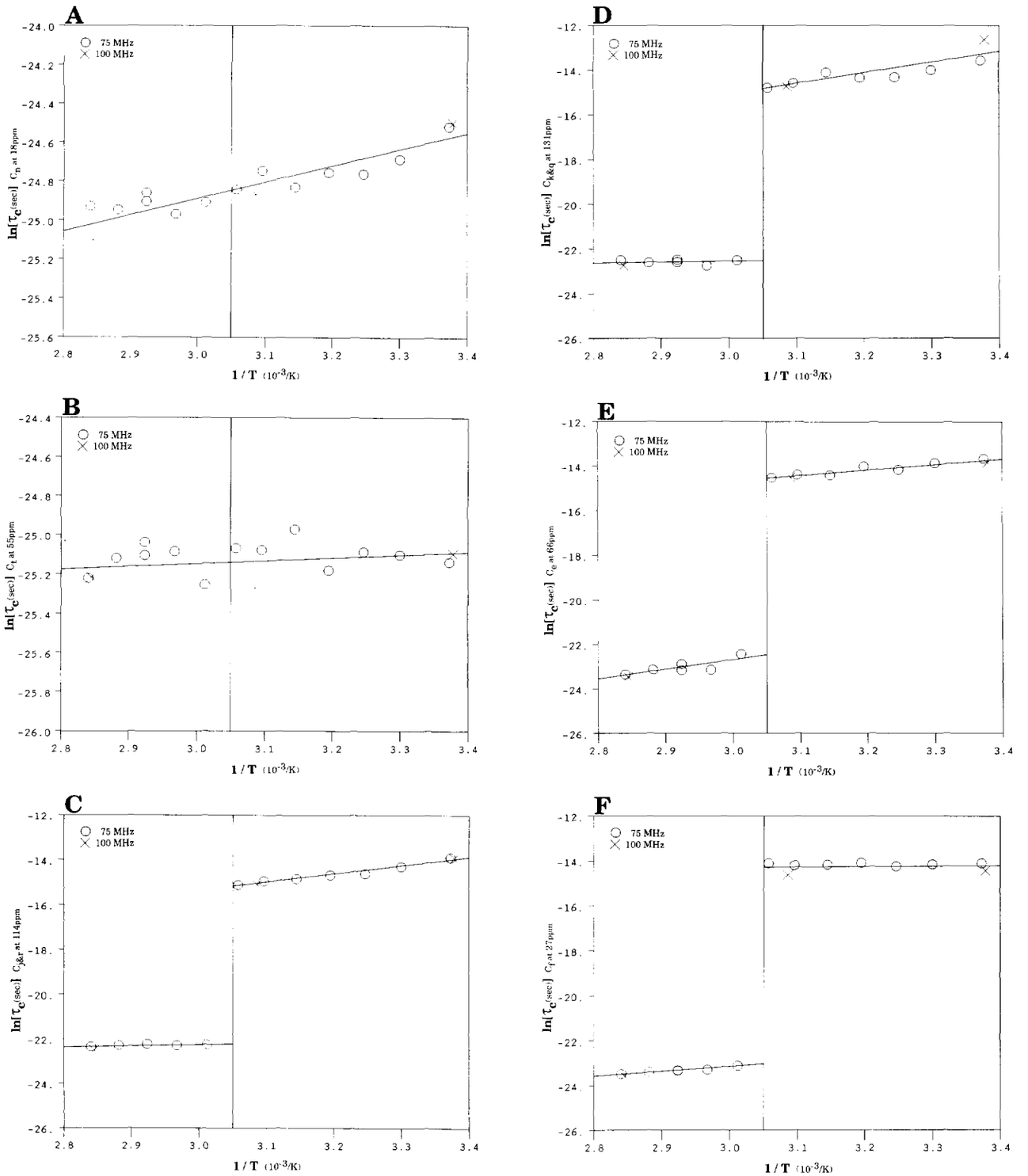


**Figure 5** Arrhenius plots of the natural logarithm of the correlation time as a function of inverse temperature at 75 and 100 MHz for (A) the peak at 18 ppm assigned to $C_n$, (B) the peak at 55 ppm assigned to $C_t$, (C) the peak at 114 ppm assigned to $C_j$ and $C_r$, (D) the peak at 131 ppm assigned to $C_k$ and $C_q$, (E) the peak at 66 ppm assigned to $C_e$, (F) the peak at 27 ppm assigned to $C_f$, and (G) the peak at 30 ppm assigned to $C_g$ and $C_h$

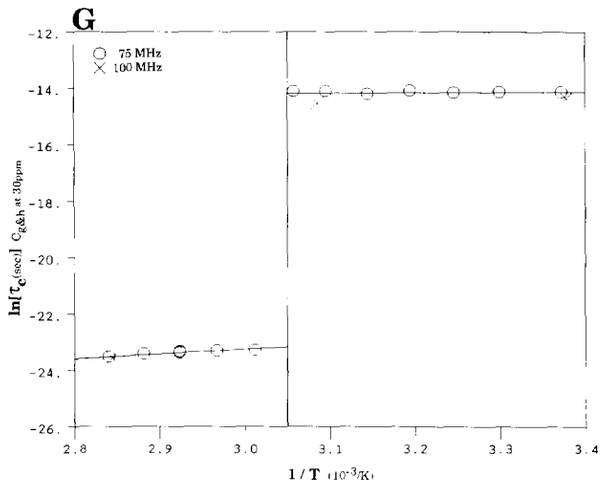


**Figure 5** *continued*

carbon. Furthermore, the $\gamma$ and $\delta$ spacer carbons, $C_g$ and $C_h$, respectively, are more mobile than the $\beta$ carbon. The $\alpha$ spacer carbon is nearly as rigid as the mesogen. The spacer begins to function as a flexible free spacer at the $\beta$ position, with further flexibility being introduced at the $\gamma$ and $\delta$ positions. Similarly, in the nematic state the mobility increases from the $\alpha$ position inward. However, the differences are not as drastic as in the nematic state.

These results are in excellent agreement with a study that we have previously published for an analogous LCP with a spacer of three methylenic units, i.e. 4′-3-PMA, in the glass state[5]. For the LCP with three methylenic units, the $\alpha$ spacer carbon was nearly as rigid as the mesogen and the $\beta$ position was 30 times more mobile[5,6].

In general, mesomorphic properties are not observed in side-chain LCPs as bulk solids when the spacer has only two methylenic units. We offer our observation here that the spacer becomes flexible at the $\beta$ position as an explanation for this.

For all four spacer carbons, $C_e$, $C_f$, $C_g$ and $C_h$, the activation energy is higher in the nematic state than in the glass state. This result is quite curious in view of the fact that the mesogen is more mobile in the nematic state. However, the motion of the mesogen that has been measured (MHz) is most likely to be ring flipping, and certainly not bending, splaying, or twisting (kHz). The regular alignment of the mesogen in the nematic state prevents the spacer from achieving certain conformations. This restricts the motion of the spacer increasing its activation energy. In addition, the high activation energy of the spacer in the nematic state may originate from the backbone end of the spacer, in view of the fact that the activation energy of the backbone increases in the nematic state. However, it is not possible to resolve the chemical shifts of the two $\alpha$ carbons, the two $\beta$ carbons, etc., i.e. the chemical shift of the carbon $\alpha$ to the backbone is overlapping with the chemical shift of the carbon $\alpha$ to the mesogen, etc. Furthermore, since the relaxation data for a particular peak fit to a single value of $T_1$, it must be assumed that both $\alpha$ carbons do indeed have the same $T_1$, i.e. if the two overlapping resonances had different values for $T_1$, then the relaxation data for that peak would fit to a two-component exponential equation.

*Activation energies for backbone carbons*

In the glass state, the activation energy of the quaternary carbon in the backbone, $C_b$, at 45 ppm, is lower than that of the mesogen. However, the activation energy of the main-chain backbone increases in the nematic state and is greater than that of the mesogen. It has been widely thought that the backbone acts as a viscous drag to the motion of the mesogen, i.e. a mesogen is capable of liquid-like flow, but its motion is hindered because it is attached to a high viscosity polymeric backbone. In the glassy state the backbone is not a viscous drag, as the mesogen has a higher activation energy. Nonetheless, in the nematic state when the mesogen is capable of flow, the backbone does act as a drag to the motion of the mesogen.

*Spacer length*

*Table 3* compares the activation energies of 4′-8-PMA in the glass state to the activation energies previously published[5] for 4′-3-PMA, an analogous LCP with a spacer of three methylenic units. The carbons for 4′-3-PMA have been renamed from the previous publication, by adapting the convention used herein. The activation energies are larger for 4′-8-PMA than for 4′-3-PMA for the motion of the mesogen, the $\alpha$ spacer carbon and the $\beta$ spacer carbon. Therefore, in the glass state the respective carbons are more rigid when the spacer is longer.

It has been widely thought that a longer spacer is more effective in separating the motion of the mesogen from that of the backbone. One should be careful not to conclude from the activation energies that the longer spacer is less effective in separating the motion of the mesogen from that of the backbone. The activation energies given herein are limited to motions in the MHz frequency regime; motions with slower time scales have not been characterized. In addition, the activation energies given are limited to the glass state, as motions in the liquid crystalline states have not been characterized.

*Error*

Two independent determinations of $T_1$ at 69°C and 75 MHz were used to ascertain the experimental uncertainty. The error was determined for each carbon and converted to a percentage, and this percentage was then averaged for all peaks. In this manner, the values of $T_1$ were determined to be accurate to $\pm 5\%$. The uncertainty in $T_1$ propagates to an uncertainty of $\pm 5\%$ in $\tau_c$. Furthermore, the uncertainty in $\tau_c$ propagates to an uncertainty of $\pm 1\%$ in $E_a$.

At a given temperature, values of $\tau_c$ at two field strengths should be almost equal because the spectral density function is smooth[2-4]. Using all peaks at the three

**Table 3** Comparison of activation energies in the glass state for analogous LCPs with spacers of three[5] and eight methylenic units

| | $E_a$ (kJ mol$^{-1}$) | |
|---|---|---|
| Carbon | 4′-3-PMA | 4′-8-PMA |
| $C_d$, $C_f$ | 7.1 | 32.1 |
| $C_e$ | 3.2 | 21.1 |
| $C_f$ | 0.1 | 0.709 |

temperatures that were run at both field strengths, an error of $\pm 10\%$ was determined for $\tau_c$. This uncertainty in $\tau_c$ includes (a) the experimental error and (b) the error caused by lack of fit of the model used to analyse the data. The model chosen assumes (a) pure $^{13}C$–$^{1}H$ dipolar relaxation (equation (3)) and (b) random isotropic reorientation of the C–H vector, thus leading to a single correlation time (equation (4)).

The total error of $\pm 10\%$ for $\tau_c$ includes (a) the experimental error and (b) the error caused by lack of fit of the model. The experimental uncertainty in $\tau_c$ is $\pm 5\%$. Therefore, the error in the fit of the model is 5%. Given such a small error for the fit of the model, there is no need to adapt any of the more complex spectral density functions that have been previously proposed[18].

## CONCLUSIONS

$^{13}C$ n.m.r. spin–lattice relaxation data in the solid state are effectively modelled by dipolar relaxation (equation (3)) and random isotropic motion (equation (4)).

For the methyl carbons $C_n$ and $C_t$, $T_1$ at 75 MHz is equal to $T_1$ at 100 MHz over the entire temperature range. The methyl groups spin rapidly about their $C_3$ axis on the fast side of the $T_1$ minimum. Furthermore, the activation energy for the spinning of a methyl group does not change at the phase transition.

For all other carbons, in the glassy state, $T_1$ at 100 MHz is larger than $T_1$ at 75 MHz, while in the nematic state $T_1$ at 100 MHz is equal to $T_1$ at 75 MHz. The glassy polymer undergoes motions on the slow side of the $T_1$ minimum. At the phase transition the correlation times jump three to four orders of magnitude and the nematic LCP undergoes motions on the fast side of the $T_1$ minimum.

The motional activation energies of all three sites in the mesogen are almost equal in the glass state, indicating that there is one single collective motion. The activation energy decreases by a factor of 6 in the nematic state as the LCP is no longer frozen. Again, in the nematic state all three sites on the phenyl ring have nearly equal activation energies.

In the glassy state the activation energy of the $\alpha$ spacer carbon is nearly equal to that of the mesogen, while the $\beta$ spacer carbon is 30 times more mobile. The spacer begins to function as a flexible free spacer at the $\beta$ position, thus supporting previously published results[5]. Further flexibility is introduced at the $\gamma$ and $\delta$ positions. Likewise, in the nematic state the mobility increases from the $\alpha$ position inward.

The activation energy of the backbone increases in the nematic state, and the backbone acts as a viscous drag to the motion of the mesogen.

Comparing the LCP with a spacer of eight methylenic units to the LCP with a spacer of three methylenic units[5], $E_a$, in the glass state, is larger for 4′-8-PMA than for 4′-3-PMA for the motion of the mesogen, the $\alpha$ spacer carbon and the $\beta$ spacer carbon.

## ACKNOWLEDGEMENTS

Special acknowledgement is given to Professor Virgil Percec and Dr Dimitris Tomazos from the Department of Macromolecular Science, Case Western Reserve University, for supplying the liquid crystalline polymers and monomers. Funding was provided by the Materials Research Group and the National Science Foundation.

## REFERENCES

1 Noël, C. and Navard, P. *Prog. Polym. Sci.* 1991, **16**, 55
2 Koenig, J. L. 'Spectroscopy of Polymers', American Chemical Society, Washington DC, 1992
3 Bovey, F. A. and Jelinski, L. W. *J. Phys. Chem.* 1985, **89**, 571
4 Perry, B. C. and Koenig, J. L. *J. Appl. Polym. Sci. Appl. Polym. Symp.* 1989, **43**, 165
5 Silvestri, R. L. and Koenig, J. L. *Macromolecules* 1992, **25**, 2341
6 Silvestri, R. L. *MS Thesis* Case Western Reserve University, Cleveland, 1991
7 Perry, B. C., Hahn, B., Percec, V. and Koenig, J. L. *Polymer* 1990, **31**, 721
8 Yoshizawa, A., Kikuzaki, H., Hirai, T. and Yamane, M. *Jpn J. Appl. Phys.* 1990, **29**, 64
9 Hutton, H., Bock, E., Tomchuk, E. and Dong, R. Y. *J. Chem. Phys.* 1978, **68**, 940
10 Schwartz, M., Fagerness, P. E., Wang, C. H. and Grant, D. M. *J. Chem. Phys.* 1974, **60**, 5066
11 Kumagai, M., Soda, G. and Chihara, H. *J. Magn. Reson.* 1981, **42**, 28
12 Hayamizu, K. and Yamamoto, O. *Bull. Chem. Soc. Jpn* 1977, **50**, 1295
13 Laupretre, F. *Prog. Polym. Sci.* 1990, **15**, 425
14 Fukushima, E. and Roeder, S. B. W. 'Experimental Pulse NMR: A Nuts and Bolts Approach', Addison-Wesley, Reading MA, 1981
15 Farrar, T. C. 'An Introduction to Pulse NMR Spectroscopy', Farragut Press, Chicago, 1989
16 Becker, E. D. and Fisk, C. L. in 'NMR in Living Systems' (Eds T. Axenrod and G. Ceccarelli), D. Reidel, Boston MA, 1986
17 Doddrell, D., Glushko, V. and Allerhand, A. *J. Chem. Phys.* 1972, **56**, 3683
18 Dejean de la Batie, R., Lauprêtre, F. and Monnerie, L. *Macromolecules* 1988, **21**, 2045
19 Chen, Q., Yamada, T., Kurosu, H., Ando, I., Shiono, T. and Doi, Y. *J. Polym. Sci. Polym. Phys. Edn* 1992, **30**, 591
20 Bull, L. M., Gillies, D. G., Matthews, S. J., Sutcliffe, L. H. and Williams, A. J. *Magn. Reson. Chem.* 1991, **29**, 273
21 Percec, V. and Tomazos, D. *Macromolecules* 1989, **22**, 2062
22 Frye, J. S. and Maciel, G. E. *J. Magn. Reson.* 1982, **48**, 125
23 Monnerie, L. *Pure Appl. Chem.* 1985, **57**, 1563
24 Monnerie, L., Lauprêtre, F. and Noël, C. *Liq. Cryst.* 1988, **3**, 1013
25 Aklonis, J. J. and MacKnight, W. J. 'Introduction to Polymer Viscoelasticity', 2nd Edn, Wiley, New York, 1983
26 Silverstein, R. M., Bassler, G. C. and Morrill, T. C. 'Spectrometric Identification of Organic Compounds', 5th Edn, Wiley, New York, 1991
27 Breitmaier, E. and Bauer, G. '$^{13}C$ NMR Spectroscopy: A Working Manual', Harwood Academic, New York, 1984
28 Earl, W. L. and VanderHart, D. L. *J. Magn. Reson.* 1982, **48**, 35
29 Grinsted, R. A., Silvestri, R. L. and Koenig, J. L., unpublished results
30 Grinsted, R. A. *PhD Thesis* Case Western Reserve University, 1991
31 Fung, B. M. and Gangoda, M. *J. Chem. Phys.* 1985, **83**, 3285
32 Grant, D. M. and Cheney, B. V. *J. Am. Chem. Soc.* 1967, **89**, 5315
33 Tonelli, A. E. 'NMR Spectroscopy and Polymer Microstructure: The Conformational Connection', VCH, New York, 1989
34 Gerstein, B. C. and Dybowski, C. R. 'Transient Techniques in NMR of Solids', Academic, New York, 1985
35 Müller, K., Wassmer, K. H. and Kothe, G. *Adv. Polym. Sci.* 1990, **95**, 1
36 Galland, D., Gerard, H., Ratto, J. A., Volino, F. and Ferreira, J. B. *Macromolecules* 1992, **25**, 4519
37 Volino, F., Galland, D., Ferreira, J. B. and Dianoux, A. J. *J. Mol. Liq.* 1989, **43**, 215